



ELSEVIER

Available online at www.sciencedirect.com

SCIENCE @ DIRECT®

Nuclear Instruments and Methods in Physics Research A 545 (2005) 705–715

NUCLEAR
INSTRUMENTS
& METHODS
IN PHYSICS
RESEARCH
Section A

www.elsevier.com/locate/nima

A test of silicon photomultipliers as readout for PET

A.N. Otte^{a,*}, J. Barral^b, B. Dolgoshein^c, J. Hose^a, S. Klemin^d, E. Lorenz^a,
R. Mirzoyan^a, E. Popova^c, M. Teshima^a

^aMax Planck Institute for Physics, Föhringer Ring 6, 80805 Munich, Germany

^bEcole Polytechnique, 91128 Palaiseau, France

^cMoscow Engineering and Physics Institute, Kashirskoe Shosse 31, 115409 Moscow, Russia

^d“Pulsar” Enterprise, Okružhnoj Proezd 27, Moscow, Russia

Received 1 February 2005; received in revised form 22 February 2005; accepted 22 February 2005

Available online 15 April 2005

Abstract

The silicon photomultiplier (SiPM) is a novel photon detector based on Geiger mode operating avalanche photodiodes. In this paper, we present results from a test, demonstrating the feasibility of SiPM as readout elements in scintillator-based positron emission tomography (PET). As scintillator we use the newly developed LYSO crystals having similar characteristics as LSO. With our setup we measure an energy resolution of about 22% and a time resolution of a single crystal element of (1.51 ± 0.07) ns, both full-width at half-maximum. A significant improvement in time resolution could be achieved by triggering on the first photoelectron in the signal. We also present the coincidence rate of two detector channels vs. the position of a small point-like ^{22}Na positron source.

© 2005 Elsevier B.V. All rights reserved.

PACS: 29.30.Kv; 29.40.-n; 85.60.Dw; 85.60.Gz; 87.58.Fg

Keywords: Positron emission tomography (PET); Silicon photomultiplier (SiPM); Lutetium yttrium orthosilicate (LYSO); Avalanche photo diode (APD)

1. Introduction

Positron emission tomography (PET) scanners are powerful tools for the study of physiological processes in vivo. Current developments aim to

build smaller, more compact and less expensive devices with improved resolution and a simpler mode of operation. In case of higher spatial resolution, respectively, finer structures, one has to take into account the body movements to make the correct correlation with anatomical structures. It might be of advantage to combine a PET scanner with an NMR scanner in order to simultaneously acquire information about the

*Corresponding author. Tel.: +49 89 32354259;

fax: +49 89 32354516.

E-mail address: otte@mppmu.mpg.de (A.N. Otte).

morphological structure and physiological processes. To comply with these requirements, a reliable and cheap photon detector is needed, which is insensitive to magnetic fields and pickup as well as causing minimal interference with the NMR detector's data acquisition system.

The so-called silicon photomultiplier (SiPM) is a novel approach towards an inexpensive high efficient photon detector that is developed by several groups [1–3]. First suggestions to use SiPMs as photon sensor in PET applications can be found in e.g. [4], but no specific study had been performed at that time. We have carried out such a study and presented first results in Ref. [5]. There we came to the conclusion that SiPMs can in principle be used for scintillating crystal readout in PET detectors. Since then we have improved our experimental setup to demonstrate the full feasibility of using SiPMs in PET.

This paper has the following structure. Firstly, we give a short introduction to the working principle of SiPMs. Then we discuss our setup and present experimental results on energy, time and position resolution. Finally, we conclude on the prospects of SiPMs in PET and discuss some special issues and advantages of the SiPM as readout element.

2. The silicon photomultiplier

A SiPM is composed of an array of small avalanche photodiodes (APD) combined to form a macroscopic unit (typically 500 to 4000 APDs per mm^2); see Fig. 1 for the basic concept. In the following, we refer to the individual array element as 'cell', while we name the macroscopic unit a 'pixel' or SiPM. Each cell operates in limited Geiger mode, i.e. a few Volts above breakdown voltage. In this mode of operation, an electron initiates an avalanche breakdown confined to a cell (the electron 'triggers' the cell). A small polysilicon resistor, which connects the cell to a conductive grid on the front side (see Fig. 2), limits the current through the junction and eventually quenches the avalanche once the cell capacity has been discharged.

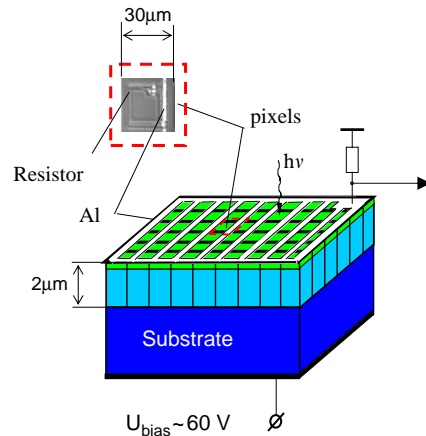


Fig. 1. Isometric view of a simplified SiPM. Light is incident from the top. The small inset shows a picture of one of the cells of which the SiPM is composed of. The cell is connected via a small polysilicon resistor to the aluminum grid which serves as common readout for all cells.

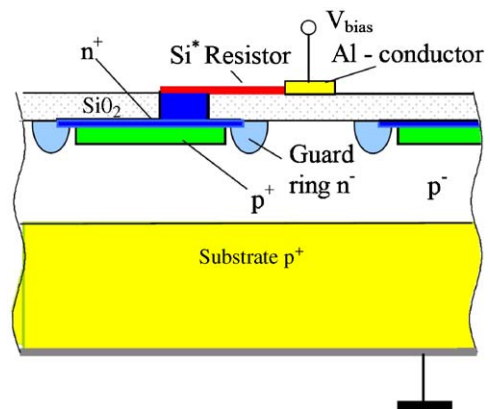


Fig. 2. Cross-section through the topology of one SiPM cell. On the right side, a part of a neighboring cell is shown. Photons are incident from the top. (Drawing taken from [6].)

For each Geiger breakdown, the output signal of a cell has always the same shape and charge (except for small variations due to differences from cell to cell introduced in the production process). It should be noted that in case two photoelectrons are produced simultaneously in a cell, the output signal is nevertheless standardized. Therefore, one cannot distinguish if one or more photoelectrons have been generated in a cell.

As mentioned above, in a SiPM the independent operating APD cells are all connected via resistors to a common readout line. Therefore, the output signal is the superposition of the standardized signals of all fired cells. In case of not too intense light flashes, the number of fired cells is in first-order proportional to the number of photons thus compensating for the missing dynamic range of a single Geiger mode APD. For large light flashes (as well as for a sizeable light background), saturation effects set in. In reality, the process is more complex because of the recovery time of the cells and the influence of dark current. The main domain of operation for SiPMs is for light levels with a photoelectron flux $\ll 1$ photoelectron/cell/recovery time. Not all photoelectrons are able to initiate an avalanche breakdown, therefore the so-called photon detection efficiency (PDE) is lower than the quantum efficiency (QE) in the photodiode operation mode of the SiPM.

In detail, the PDE of current SiPM prototypes is influenced by several contributions. The most important ones are:

- the fraction of the active area of a pixel,
- the QE of the active area,
- the probability to initiate an avalanche breakdown (Geiger efficiency),
- the fraction of active cells, i.e. those cells which are not quenched or are still recovering from a previous breakdown.

In first-order, the PDE is a product of the four quantities.

The active area fraction, limited by the dead area around each cell, depends on the construction and ranges typically between 20% and 70% of the total area. Typical values of PDE of recent SiPMs are comparable to the QE of conventional alkali photomultipliers. It is expected that the PDE of SiPMs will be increased in the near future as new ideas and promising new concepts will be investigated.

The main advantages of SiPMs compared to linear (classical) APDs are:

- standardized output pulses for single photoelectrons,

- low sensitivity for pickup, respectively, EMI,
- large intrinsic gain, 10^5 – 10^6 ,
- no need for sophisticated and expensive pre-amplifiers,
- fast pulse risetime,
- significantly lower operating voltages (20–200 V) compared to that for classical APDs or PMTs,
- more stable operation conditions compared to those of classical APDs, e.g. less stringent requirements for temperature and bias stabilization,
- the costs are expected to be rather low because of simple production techniques.

The PDE average of the SiPM is, due to the dead area fraction between the cells, much lower than that of classical APDs while the PDE of the active area of one SiPM cell is actually similar or in case of APDs with high F-factors even superior.¹ SiPM prototypes suffer from a relatively high dark rate (0.2–2)MHz/mm² at room temperature. The number of thermally generated electron–hole pairs in the sensitive volume gives the ultimate lower limit. Cooling allows one to reduce the dark count rate. For the use in PET, a high dark rate is uncritical, as one is interested in signals that exceed the one-photoelectron level by a large margin while the integration window is only a few tens of nanoseconds for fast scintillators.

3. The SiPM used in the test setup

For our studies we used a (1 × 1)mm² prototype SiPM developed at MEPhI and PULSAR enterprises. The used device has an n–on–p structure and is therefore less sensitive to the blue part of the emission spectrum of the LYSO scintillator. In the near future, new devices with a p–on–n structure and thus with enhanced blue sensitivity will be available. The characteristics of the used SiPM are summarized in Table 1. For a more detailed explanation of the sensor itself we point the interested reader to Ref. [1].

¹The PDE of classical APDs is rather complex and depends very much on the gain, respectively on the F-factor at the working point.

Table 1
Specifications of the SiPM used in this study

Parameter	Value
Sensor area	$(1 \times 1) \text{ mm}^2$
Number of individual cells	576
Active area of the sensor	25%
Peak PDE (at 540 nm)	20% [1]
Bias voltage	52 V – 60 V
Breakdown voltage	50 V
Gain	$10^4 - 5 \times 10^6$
Typical dark count rate at room temperature	$10^6 \text{ counts/mm}^2/\text{s}$

4. Experimental setup

4.1. Mechanics

We constructed a simple mechanical support from Lucite for a good fixation and coupling of the crystal and photon detector combination (see Fig. 3). In between the two crystals we placed a small ^{22}Na -source that faked a point-like positronium source. The distance between the two detectors was 5 cm.

As scintillator crystals we used LYSO, which was provided by the company Saint Gobain. The crystals have polished surfaces and dimensions $(2 \times 2 \times 15) \text{ mm}^3$. LYSO has a high light yield of 32000 photons/MeV and a fast decay time of 40 ns [7]. Each crystal is wrapped in a dielectric mirror foil from 3M to assure good light collection. The reflectivity of this prototype foil is shown in Fig. 4. The same foil with a $(1 \times 1) \text{ mm}^2$ hole is used for an aperture and is placed between the end face of the scintillator and the photon detector. This is necessary to compensate for some of the large area mismatch between the sensitive area of the SiPM (1 mm^2) and the four times larger end face of the scintillator. The light coupling between crystal and photon detector was improved by optical grease BC630 by Saint Gobain (refractive index 1.463).

4.2. Signal readout

For the explanation of the electrical signal readout we refer to Fig. 5. For most of the tests, we used an additional passive RC-integrator

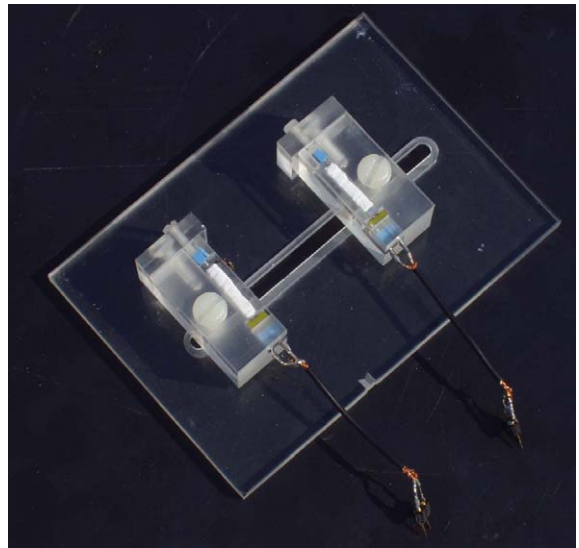


Fig. 3. Photograph of the detector setup used in this study. For details see text.

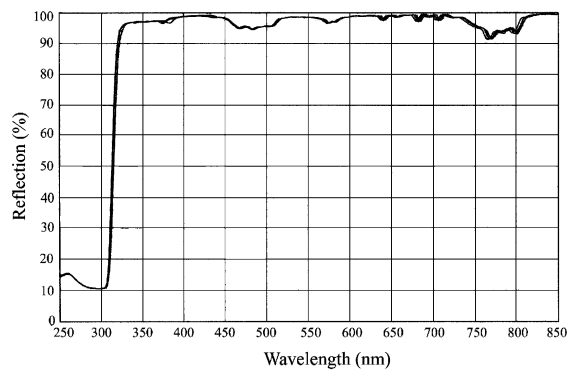


Fig. 4. Reflectivity of the dielectric foil by 3M measured at four different positions on a sample.

($\sim 1 \dots 10 \text{ ns}$) located at the SiPM in order to shape the signal. The shaped signal is routed via a Belden 50Ω coaxial cable to a preamplifier MAN-1LN from Mini Circuits. No special care was taken to further optimize the signal shape or to suppress noise.

After shaping and amplification, the signal is split by a passive divider and routed to an LC554DL oscilloscope and to the input of a discriminator. The oscilloscope is used to determine the magnitude of the signal by measuring the area under the signal trace (charge) for about

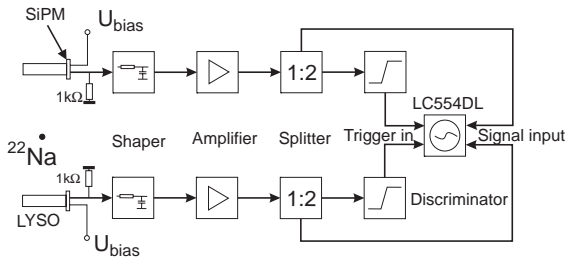


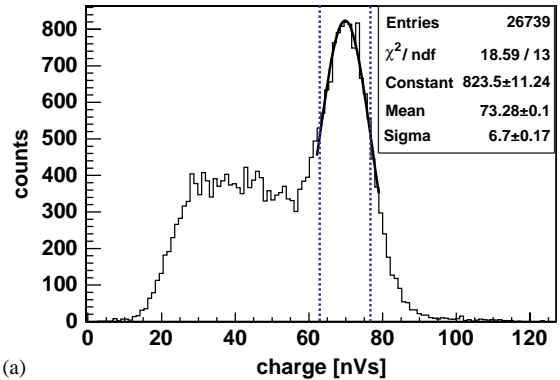
Fig. 5. Block diagram of the electronics used in this test.

300 ns for most of the measurements. The output of the discriminator is fed via another input into the LC554DL and supplies a time information. For further analysis, the time information and signal magnitude are sent via GBIP to a PC.

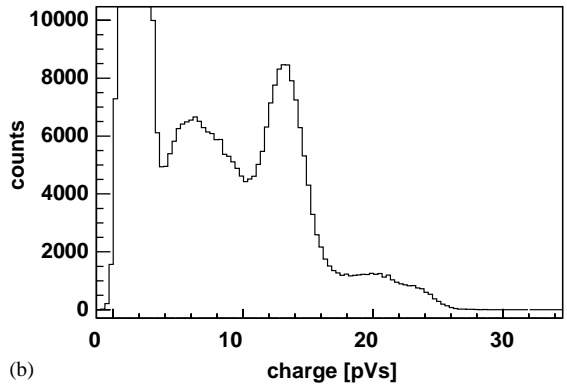
The scope was triggered by the coincidence of the two discriminators with a threshold of ~ 250 mV corresponding to a few photoelectrons.

5. Energy resolution and calibration

The pulse height distribution in Fig. 6(a) shows the γ -spectrum from the ^{22}Na source when triggering on coincidence events. The spectrum was measured with the source placed half way between the LYSO crystals. The spectrum shows the photopeak of the 511 keV- γ 's fully absorbed in the LYSO crystal and a contribution from Compton scattered events (Compton continuum). Due to the coincidence alignment condition the Compton continuum is partially suppressed and the valley between the Compton edge and the photopeak is nearly invisible. Fig. 6(b) shows the ^{22}Na spectrum in a self-triggered mode. In this case, the Compton contribution is much higher and the valley well visible. For the determination of the energy resolution, we fitted the photopeak in Fig. 6(a) by a single Gaussian and neglected the contribution from the Compton edge. We found for the photopeak a full-width at half-maximum (FWHM) of about 22%. This value, although not fully correct, is a significant improvement compared to the $(35 \pm 1)\%$ FWHM we have reported earlier [5] and is closer to the 15% FWHM reported by Pichler [8] for the APD-LSO readout.



(a)

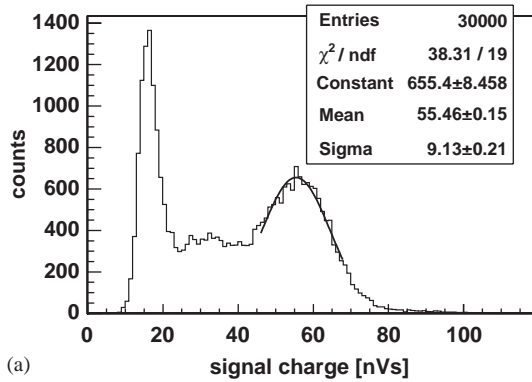


(b)

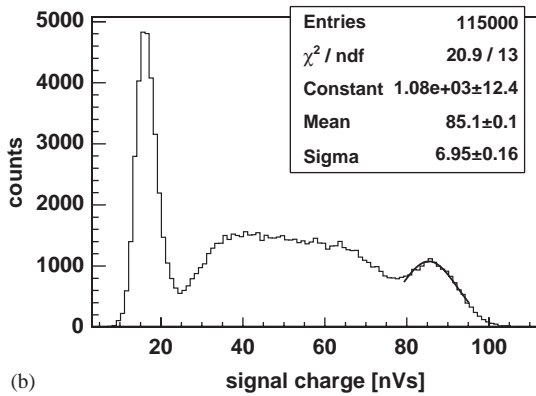
Fig. 6. Pulse height distributions of a positronium source. The distribution on the left side was measured by triggering on a coincidence of the two channels. The dashed vertical lines indicate the cuts applied in order to restrict the analysis of the time resolution to the photopeak signal. For the distribution on the right-hand side a minimum amplitude in the detector channel was required. The 511 keV peak as well the 1.275 MeV peaks are clearly visible. Note that for the right-hand picture, no amplifier and an additional attenuator (18 dB) was used. (a) with coincidence requirement and (b) without coincidence requirement.

In addition, we measured the energy-dependent resolution as well as the energy response by measuring also the pulse height distribution of a ^{133}Ba - and a ^{137}Cs -source. ^{133}Ba and ^{137}Cs emit γ 's with energies of 356 and 662 keV, respectively [9]. The resulting spectra are shown in Fig. 7.

The spectrum around the photopeak has been fitted by a Gaussian. In Fig. 8, the peak values are plotted versus the known energy. As expected, the correlation between the measured signal and the incident energy is not well described by a linear function. This can be explained by saturation



(a)



(b)

Fig. 7. Pulse height distributions of ^{133}Ba and ^{137}Cs . The peaks at lower energy are caused by dark counts where, due to crosstalk, many standardized signals are produced within $\ll 1$ ns and the summed up signal is high enough to pass the discriminator threshold. (a) ^{133}Ba pulse height distribution (356 keV γ -source) and (b) ^{137}Cs pulse height distribution (662 keV γ -source).

effects caused by the large number of fired cells in the SiPM (around 400 for the 511 keV line, as will be derived later). Also, optical crosstalk and subtle recovery time effects contribute.

The gain calibration of an SiPM is done by analyzing the pulse height distribution of the dark counts (see Fig. 9). The integration window in this measurement was reduced to 10 ns. As the output of a cell is standardized, the number of fired cells can be derived in first-order from the pulse height distribution of the dark count spectrum. We measured the gain by determining the positions of the peaks. The slope of a linear fit to the peak positions in electrons vs. the number of fired cells

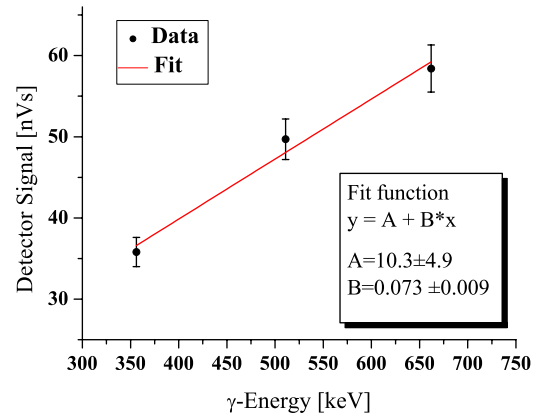


Fig. 8. Correlation between γ -energy and signal height (in units of charge, respectively, the number of fired cell).

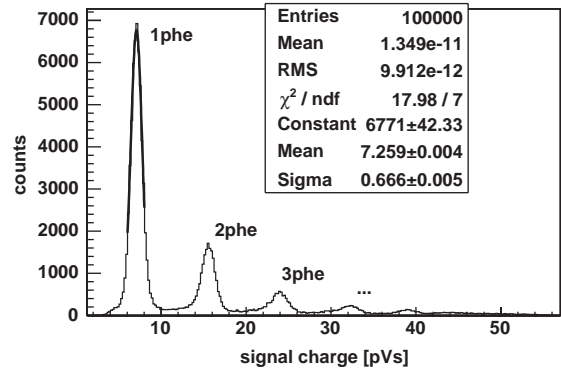


Fig. 9. Spectrum of dark count pulses in the used SiPM. Each peak corresponds to a different number of cells fired per event. The distribution was measured without any preamplifier but the passive splitter still included. The insert box lists the fit result for the first peak.

gives the gain. For our configuration we found a gain of $(2.1 \pm 0.16) \times 10^6$.

Together with the gain of the SiPM and the preamplifier (21.1 ± 0.1), we also determined the number of cells that fired on average if one 511 keV- γ was fully absorbed in the crystal. From the ^{22}Na pulse height distribution in Fig. 6(a) we calculated that the peak position corresponds to 413 ± 20 fired cells. Therefore, the signal should already in part be affected by saturation effects as the used SiPM comprises 576 cells. This conclusion is based on the assumption that the SiPM has a recovery time being significantly larger than the gate time for the charge selection.

The dependence of the SiPM signal N_{SiPM} on the number of photoelectrons N_{phe} is given by

$$N_{\text{SiPM}} = p(1 - e^{-\frac{N_{\text{phe}}}{p}}) \quad (1)$$

where p is the number of cells of the SiPM.

We want to stress again that this formula is based on the assumption that the recovery time of the fired cells is much longer than the optical decay time of the scintillator and recovery effects are therefore be neglected.

From Eq. (1), we calculate for 413 fired cells at the photopeak a mean number of ~ 730 photoelectrons. This number includes both primary photoelectrons generated by scintillation photons as well as electrons generated by optical crosstalk photons. Optical crosstalk within the SiPM leads to a higher than expected output signal as additional cells fire. The origin of optical crosstalk has been traced to secondary photons generated in the avalanche breakdown of fired cells [10]. These photons can be absorbed in neighboring cells and fire them in addition. The pulse height distribution of the dark count in Fig. 9 is a direct effect of optical crosstalk. Thus, this spectrum is the probability distribution that none, one, two, three and so on cells fire in addition to one primary fired cell. By using a simple Monte Carlo simulation (neglecting recovery effects of the cells), we corrected for the optical crosstalk. In the simulation, the crosstalk is implemented as a probability distribution, following the pulse height distribution of the dark counts. According to that distribution, the number of cells which in principle could fire in addition due to crosstalk, is determined for each primary fired cell. In a second step, every crosstalk cell is associated with a randomly picked cell of the SiPM which is then marked as fired if it has not been fired earlier. A recovery of a pixel once fired was not taken into account in the Monte Carlo.

As an outcome of that simulation, we found that the number of primary photoelectrons should have been around 520. This is in fairly good agreement with a simple estimate from the scintillation light yield of 16 650 photons for a 511 keV- γ , a typical light collection onto the SiPM of around $25 \pm 5\%$ and a mean PDE of around

12% with an estimated error of 3% (due to the spectral mismatch) of (500 ± 180) photoelectrons.

Monte Carlo simulations predict an energy resolution of 7% FWHM assuming an ideal scintillator with a Gaussian-like light distribution over time with fluctuations proportional to $\sqrt{N_{\text{phe}}}$. Even for optimal light collection, one commonly finds for high light yield scintillators that the resolution does not follow strictly the $\sqrt{N_{\text{phe}}}$ rule [11]. We conclude that the 22% resolution has its origin either in crystal scintillation non-uniformities or non-uniform light collection due to the aperture and the large area mismatch. Further studies are needed for the clarification of the 22% resolution.

6. Influence of the recovery time

Fig. 6(b) shows besides the prominent 511 keV peak indications of the 1.275 MeV line and the corresponding Compton edge (note that the photo efficiency of LYSO around 1200 keV is already highly suppressed). Using the above calibration, we find a number of fired channels exceeding 576. This can only be explained if fired SiPM cells can recover already within the gating time and are therefore sensitive to late emitted photons from the LYSO. In a simple test, the SiPM was illuminated by an intense laser pulse of very short duration and the onset of the noise rate and amplitude inspected. Already around 60 ns small noise pulses became visible with later ones increasing in amplitude. In a second test, the SiPM was illuminated first by the laser pulse to fire all cells and than illuminated by a delayed light pulse showing again the onset of a small signal after about 60 ns. After about 500 ns the full amplitude was reached. Further studies with better test equipment are needed because there might be two effects be present simultaneously. After a short delay time, the cell gain is still reduced but the avalanche probability is reduced as well. Also, optical crosstalk should be affected.

Further tests are needed but complex recovery effects have to be considered when integrating scintillation light over a duration exceeding the partial recovery. Naively speaking, the 425 fired

cells are based on the assumption of standardized cell pulses. Due to partial recovery resulting in lower cell amplitudes, the number of fired cells must be considerably larger than 425 and in turn the number of detected photoelectrons also larger than 520.

7. Time resolution

For the measurement of the time resolution, we only accepted events within the one sigma limit around the photopeak in each channel (see vertical lines in Fig. 6(a)). The selection of accepted events was done offline.

One series of tests was performed with a constant fraction (CF) discriminator triggering on the rising edge of the signal. Between the SiPM output and the preamplifier input, we inserted a passive element to shape the signal. We varied the time constant of the shaping element and the delay of the constant fraction discriminator. The best time resolution for one detector channel of (2.24 ± 0.03) ns FWHM was achieved without shaping and a delay of 7 ns. We did not correct for the time resolution of the electronics, which was 200 ps and thus can be neglected.

We also tried a different timing method by triggering on half height of the first photoelectron in the detector signal with a normal leading edge discriminator (LeCroy 621AL). Because of the well-defined single photoelectron signal of the SiPM, this is a very promising and cheaper method compared to a CF-discriminator, which is not so simple to realize as an IC. As an additional trigger condition, we required a minimum signal amplitude of a few tens of photoelectrons. In this way, we triggered only on γ 's. With this setup, we achieved a 39% improvement in time resolution compared to the constant fraction method. The distribution of the time differences between the two channels is plotted in Fig. 10. From the distribution, we derive a time resolution for a single detector channel of (1.51 ± 0.07) ns FWHM. This is comparable to the CF timing in classical APD-LSO combinations in PET [12]. The very similar resolution with a SiPM where one detects even less than 20% of the photoelectrons com-

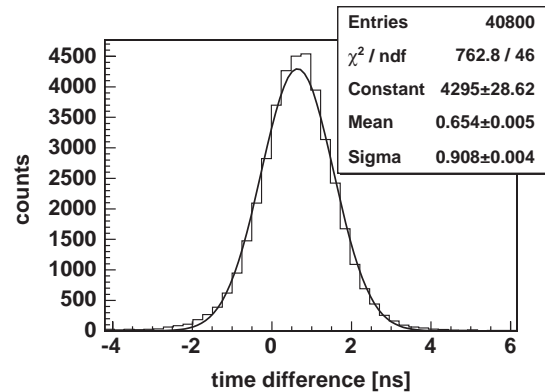


Fig. 10. Distribution of time differences of the two detector channels. For this measurement, the time was measured by triggering on the first photoelectron of each signal with a leading edge discriminator.

pared to an APD can be explained by the fact that one triggers in SiPMs on the well-shaped signal of the first photoelectron.

8. Position resolution

The sensitivity of the detector setup on the position of the ^{22}Na γ -source was tested by measuring the coincidence rate versus the displacement of the γ -source. For this test, we set the distance between the two crystals to 5 cm and placed the radioactive sample in between. Then we moved the ^{22}Na sample perpendicular to the long side of the crystals. The result is shown in Fig. 11. One expects a linear rise and fall of the coincidence rate as the source moves through the setup. The expected behavior is nicely reproduced by our measurement. The FWHM of the coincidence rate is 1 mm, i.e. only limited by the size of the crystals.

9. Conclusions and discussion of the results

In this study, we have confirmed the good prospects of using SiPMs as new photon detectors in PET.

In detail the following conclusions can be drawn from the studies:

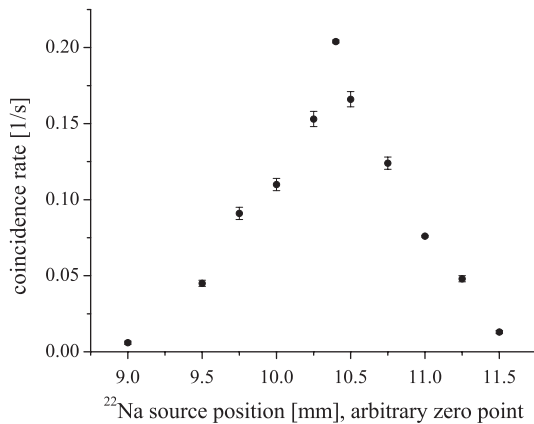


Fig. 11. Coincidence rate as function of the ^{22}Na γ -source position.

- (1) The 511 keV- γ energy resolution of about 22% FWHM was found to be somewhat worse compared to that achieved with larger classical APDs with a 1:1 coupling to small crystals. The achieved energy resolution is remarkable, as the scintillator was coupled to a SiPM, which is four times smaller than the end-face of the crystal, and the 511 keV- γ signal corresponds on average to about 500 photoelectrons. Nevertheless, there remains a discrepancy between the resolution predicted by Monte Carlo simulations and the observed value. We explain this mainly by either
 - a non-uniform light yield of the tested crystals originating in part from the inhomogeneous cerium doping in the crystals
 - by some uneven light collection at the end close to the SiPM
 - by possibly a contribution of the dead time recovery effects.

The first deficiency can be improved by growing crystals at different parameters while the second problem can normally be solved by a mix of diffuse and specular reflectors and a larger SiPM.

- (2) The impact of recovery of the fired cells is not fully understood and needs more studies. Simple measurements show that cells start to become again sensitive within less than

60 ns, i.e. while the LYSO crystals still emits light. The signals after a few decades of nanoseconds are not as large as the standardized ones and their amplitude recovers with the time gap between refiring. The probability of a second avalanche breakdown is likely reduced in the early phase of recovery.² The impact of recovery and the dependence of gain and avalanche breakdown as a function of delay need further studies and a better understanding for the light detection when the scintillator emission decay time is comparable to the recovery time. Nevertheless, the effect does not at all prevent the use of SiPMs in PET applications.

- (3) Provided one can tolerate some degradation of the optimal energy resolution, the use of SiPMs of much smaller area than the crystal end faces offers room for easy wiring in case of large matrices of pixels. The use of the aperture defining end reflector results only in a small loss of photons. Obviously, one should choose a SiPM with a cell number exceeding significantly the number of expected photoelectrons (possible disadvantages are an increased dead area and in turn a lower PDE. Thus optimization is required).
- (4) Quite some improvement in resolution should also be possible when using p-on-n structures with better-matched spectral sensitivity and higher PDE in the blue wavelength region. A PDE of $\geq 35\%$ is not excluded in future designs.
- (5) The reduction in dead area between cells might result in a higher crosstalk rate. This is uncritical for the use in PET. For other applications, this might require other measures to reduce the chance of avalanche-generated photons to pass into other cells such as optical separators or designs that can be operated efficiently at lower gains. A simple signal amplification per pixel, possibly

²From our measurements we concluded initially that about 420 cells have fired for a γ of 511 keV. Due to the above-described recovery and the smaller amplitudes, we conclude that in reality more cells fired and the number of photoelectrons is significantly larger than 500.

integrated on the chip, might be sufficient to work with a gain, say $5 \times 10^4 \dots 10^5$.

- (6) As mentioned above, the high noise rate is irrelevant for PET applications. Even at 1 MHz dark count rate/1 mm² SiPM, a signal of a few hundred fired cells is not at all influenced. Cooling for noise reduction is unnecessary.
- (7) The high intrinsic gain of 10^5 – 10^6 is a big advantage for PET applications. As a result of the high gain, the detector will be much less sensitive to pickup. Compared to devices using classical APDs the noise immunity is typically 2–4 orders of magnitude better. Therefore, the shielding requirements are much less demanding. This is of quite some importance when installing a PET detector inside an NMR detector where space is at a premium and where conductive installations should be avoided. It should be possible to install only the crystals and SiPMs inside the NMR magnet and connect them to the outside electronics by thin coax cables carrying both the bias voltage and the fast signals. The high gain of the SiPMs might be sufficient to drive low-power Vertical Cavity Laser Diodes (VCSEL) and transmit the analog signals by thin optical fibers to the outside electronics.
- (8) When using simple leading edge discrimination on the first photoelectron, the achieved timing resolution of 1.5 ns FWHM for a 511 keV- γ matches that achieved with linear mode APDs triggering a constant fraction discriminator. As mentioned, a leading edge discriminator is much easier to realize as an IC than a constant fraction discriminator. In principle a sub-nanosecond time resolution should be possible in case SiPMs with a larger number of pixels and a higher PDE are used. We iterated that efficient leading edge triggering is possible due to the large standardized signals of single cells.
- (9) In this test, we studied the 1:1 coupling of small crystals to small SiPMs. In principle, it should be possible to read out also ‘block’ detectors by means of larger area SiPMs. But the lower costs for the ‘1:1’ detectors and the

simpler electronics offset very much gains achieved in a lower number of larger SiPMs and a more complex analysis procedure.

- (10) Larger prototype SiPMs with sizes up to $(3 \times 3$ or $5 \times 5)$ mm² are soon available, as well as p–on–n structures. We expect from future tests to match fully the energy and timing resolution of optimized classical APD–LYSO/LSO PET elements.

In summary, we conclude that the SiPM is a photon detector concept, which, although in its prototype phase, can already fully replace classical APDs and conventional PMTs in PET. For the combination of PET with NMR, the SiPM has the advantages of:

- insensitivity to magnetic fields,
- easy gain calibration due to single cell resolution,
- low sensitivity to pickup,
- compactness,
- need of minimal electronics inside the magnetic field.

Moreover, the production costs of SiPMs are already much lower compared to other photon detectors thus a significant price reduction for PET devices is expected.

The apparent drawbacks such as modest photon detection efficiency, high dark count rates and optical crosstalk only play a minor role in PET.

Acknowledgements

The authors would like to thank L. Weiss for producing the mechanical support for the crystal SiPM combination. The LYSO crystals and optical grease were provided by F. Kniest from Saint Gobain. We are grateful that S. Rodriguez was carefully reading and correcting this manuscript. I. Wacker was so kind to scan and prepare the reflectivity measurements of the 3M foil.

References

- [1] B. Dolgoshein, et al., Nucl. Instr. and Meth. A 504 (2003) 48.
- [2] D. Bisello, et al., Nucl. Instr. and Meth. A 367 (1995) 212.
- [3] V. Golovin, et al., Nucl. Instr. and Meth. A 518 (2004) 560.
- [4] A.V. Akindinov, et al., Nucl. Instr. and Meth. A 387 (1997) 231.
- [5] N. Otte, et al., Nucl. Phys. B (Proc. Suppl.) (2004), to be published.
- [6] P. Buzhan, et al., ICFA (Fall, 2001), <http://www.slac-stanford.edu/pubs/icfa/>
- [7] Saint Gobain <http://www.saint-gobain.com>.
- [8] B. Pichler, et al., IEEE Trans. Nucl. Sci. NS-48 (2001) 1391.
- [9] S. Eidelman, et al., Phys. Lett. B 592 (1) (2004).
- [10] A. Lacaita, et al., IEEE Trans. Electron. Dev. ED-40 (3) (1993) 577.
- [11] W.W. Moses, Nucl. Instr. and Meth. A 487 (2002) 123.
- [12] B. Pichler, et al., Phys. Med. Biol. 49 (2004) 4305.